JOURNAL of
MATERIALS and MECHATRONICS:A

e-ISSN 2717-8811
JournalMM, 2023, 4(2), 571-587
https://doi.org/10.55546/jmm.1375777

Araştırma Makalesi / Research Article

Response Surface Modeling of Material Removal and Tool Wear Rate in Powder Mixed Electrical Discharge Machining of CoCrMo Alloy

Faruk ÇAVDAR[1*], CAN YILDIZ[2], Erdoğan KANCA[3]

[1] Osmaniye Korkutata University, Osmaniye Vocational School, Department of Machinery and Metal Technologies, Osmaniye, Turkey,
ORCID ID: https://orcid.org/0000-0002-4981-6428, farukcavdar@osmaniye.edu.tr
[2] Iskenderun Technical University, Institute of Graduate Studies, Hatay, Turkey,
ORCID ID: https://orcid.org/0000-0001-5289-2520, canyildiz33@gmail.com
[3] Iskenderun Technical University, Faculty of Engineering and Natural Sciences, Department of Mechanical Engineering, Hatay, Turkey,
ORCID ID: https://orcid.org/0000-0002-7997-9631, erdogan.kanca@iste.edu.tr

Geliş/ Received: 13.09.2023; **Kabul / Accepted:** 13.12.2023

ABSTRACT: Electric discharge machining (EDM) is commonly used in implant manufacturing due to the challenge of machining materials that are widely employed in these applications. The study applies response surface methodology to model the impact of powder concentration and machining parameters in powder mixed EDM of CoCrMo alloys, a prevalent material for implantation. AISI 316L stainless steel was selected as the electrode material, while Ti6V4Al was chosen as the additive powder based on their biocompatibility properties. An experimental design was created using a Taguchi L_{16} array, which involved selecting 4 levels for each parameter of additive ratio, discharge current, pulse on time, and pulse off time. Regression models were developed for material removal rate (MRR) add tool wear rate (TWR) with satisfactory coefficients of determinations (0.87). Effect of the process parameters on MRR and TWR were analysed by means of 3D response surface plots. As a result of the modeling, it was revealed that discharge current, puls on time positively affected MRR, powder concentrations and puls off time negatively affected it. On the other hand, all of the considered process parameters have increasing effect on TWR.

Keywords: Electric Discharge Machining, CoCrMo, Powder Mixed EDM, MRR, TWR, RSM

*Sorumlu yazar / Corresponding author: farukcavdar@osmaniye.edu.tr

Bu makaleye atıf yapmak için /To cite this article

Çavdar, F., Yıldız, C., Kanca, E. (2023). Response Surface Modeling of Material Removal and Tool Wear Rate in Powder Mixed Electrical Discharge Machining of CoCrMo Alloy. Journal of Materials and Mechatronics: A (JournalMM), 4(2), 571-587.

1. INTRODUCTION

Electric Discharge Machining (EDM) is regarded as the more efficient approach due to its implementation of thermal energy rather than mechanical energy for shaping of electrically conductive substances (Ceritbinmez and Kanca, 2021). In EDM, workpiece machinability is not dependent on the mechanical strength and the temperature resistance. In addition, in EDM, no intimate contact exists between the electrode and the workpiece, eliminating mechanical stresses, vibrations, and noise. EDM is widely used, especially in industries such as mold making, casting, automotive, aerospace, and surgical components, where high mechanical and thermal resistance materials and complex-shaped parts are employed (Ho and Newman, 2003; Sharma and Singh, 2014; Ceritbinmez and Kanca, 2022; Srivastava et al., 2023).

Despite its mentioned advantages, the industrial use of EDM has been limited due to disadvantages such as low processing efficiency and poor surface quality (Ceritbinmez et al., 2023). Extensive research has been conducted to overcome these disadvantages, better understand processing parameters, and improve processing performance (Mujumdar et al., 2015; Abdudeen et al., 2020). In this context, one of the methods developed in recent years to enhance the capabilities of EDM and eliminate its drawbacks is the powder mixed electro-discharge machining (PM-EDM) process. This new method, addresses the drawbacks of EDM and enhances its processing capabilities (Abbas et al., 2020).

In this method, conductive particles such as copper, graphite, tungsten, aluminum, and chromium are added to the dielectric fluid used in conventional EDM. The introduction of these particles weakens the electrical insulation properties of the dielectric fluid, which in turn reduces the spark gap between the electrode and the workpiece, thus making the EDM process more stable. This results in an increase in material removal rate (*MRR*) and surface quality of the workpiece. Additionally, some studies have found that surfaces obtained with PM-EDM exhibit high resistance to corrosion (Sharma and Singh, 2014; Rajkumar and Vishwakamra, 2018; Jawahar et al., 2019).

In recent times, the use of PM-EDM in the field of biomedicine has gained significant attention. PM-EDM is one of the most prominent shaping techniques in this sector (Rajkumar and Vishwakamra, 2018; Erdem and Kiliç, 2020; S. S. Kumar et al., 2020). The use of PM-EDM processing has been found to increase the material's corrosion and wear resistance, as well as enhance the mechanical strength and fatigue life of implants (Al-Amin et al., 2021; Zhang et al., 2022). Additionally, there have been recent reports regarding the use of PM-EDM for applying a nano-porous and bio-mimetic layer to the processed implant surface (Peng et al., 2010; Yang and Huang, 2010; Bains et al., 2020;). This coating layer promotes a strong bone-implant connection (Al-Amin et al., 2020).

CoCrMo alloy is a preferred material for orthopedic implants (Öztürk et al., 2006; Long and Rack, 1998;). This alloy is chosen for its compatibility with bone and other tissues, biocompatibility, and mechanical durability. Furthermore, CoCrMo alloy is suitable for use in corrosive environments such as bodily fluids due to its high corrosion resistance (Jakobsen et al., 2010; Onderka et al., 2014; Bahçe et al., 2019).

The electro-erosion machining method offers advantages in processing CoCrMo alloys due to its flexibility and its ability to overcome challenges associated with traditional machining methods (Kumar 2018; Cakiroglu, 2022; TRAJER, 2023). There is a substantial quantity of literature on the machining of CoCrMo alloy using EDM, both with and without the inclusion of powder in dielectric fluid. In these studies, the classic EDM processing of CoCrMo material has been examined to determine the effects of various processing parameters, electrode types, and dielectric fluids on

surface properties, biological responses, corrosion resistance, in vitro compatibility, electrochemical properties, and surface cytocompatibility of the workpiece. Graphite, W, Cu, Cu-W, and Ti have been used as electrode materials in some of these studies (Iranmanesh et al., 2017; Mahajan et al., 2019; Mahajan and Sidhu, 2019a; Mahajan and Sidhu, 2019b; Chakmakchi et al., 2021). Additionally, in other research, the impact of adding Fe2O3 and γ-Fe2O3 nano powders to the dielectric fluid at different concentrations on the MRR has been investigated (Elsiti et al., 2017; Elsiti and Noordin, 2017).

In this study, the main focus has been on ensuring that there are no residues that can be harmful to the living body on the workpiece when processing CoCrMo material using PM-EDM, especially for implant applications. Therefore, 316L, commonly used in implant fabrication, was selected as the electrode material, and Ti6V4Al, also used in implants, was chosen as the dielectric additive powder (Kayalı and Yalçın, 2020). In a previous study, the effects of powder concentration and EDM parameters on the surface quality of workpieces were investigated when processing CoCrMo with PM-EDM (Yildiz et al., 2023). Furthermore, the use of 316L and Ti6V4Al materials as both electrodes and additive powders has not been found in the literature surveys conducted by the authors.

In this study, the effects of powder concentration (w), discharge current (I), pulse duration (T_{on}), and off time (T_{off}) parameters on the material removal rate (MRR) and tool wear rate (TWR) in the processing of CoCrMo workpieces with a 316L electrode have been analyzed by modeling using the response surface methodology. A Taguchi L_{16} experimental design was conducted using four independent variables at four different levels. Through experimental procedures conducted with the specified experimental set values, wear rates on the workpiece and tool were determined. Regression models were established using the obtained data through the response surface methodology, and the results were analyzed.

2. MATERIALS AND METHODS

The impacts of powder ratio and electric discharge parameters such as discharge current, pulse duration, and off time on the material removal rate and tool wear rate in powder-mixed electro-erosion machining were investigated in this study.

To ensure that the data obtained from a limited number of experiments adequately represent the design space, a Taguchi L_{16} orthogonal experimental design was used, with each of the four independent variables having four different levels.

In this study, ASTM F1537-11 grade CoCr28Mo6 round bar was used as the workpiece, AISI 316L was employed as the electrode material, and Dielektrikum 358 EDM oil was mixed with Ti6V4Al powder in various ratios as the dielectric fluid. Experimental samples were prepared by cutting in 10 mm thickness from a 30 mm diameter round bar then polishing the surfaces. Then processed using the experimental setup detailed in reference (Yıldız et al., 2023) with the Best-3000S ZNC EDM machine.

The parameter sets used in each experiment and the corresponding MRR and TWR values are listed in Table 1. Since the number of independent variables considered in the study is relatively large, regression models were established by using the response surface methodology to better analyze the relationships among these variables and to predict the values of dependent variables for sets of variable values for which experiments were not conducted.

2.1 Determination of *MRR* and *TWR*

To determine the material removal rate, workpiece samples were processed for 10 minutes using the EDM machine, following the specified parameters. After machining, the eroded areas of the workpieces were scanned over the diameter using a Hommel Etamic C8000 profilometer with a TKU300 model probe, as shown in Figure 1, to obtain wear profiles. For each specimen 3 scans have been performed on different diameters of machined area at equal angles, thus 3 wear profile have been obtained. Subsequently, after calculating the area of the wear profile, the adapted *a*, machining depth, as shown in Figure 2, was determined by using Equation 1. Here, A_p represents the area of the wear profile, *a* denotes the equivalent height, and l represents the length of the wear profile. This equivalent machining depth was used to calculate the volume (*V*) of material removed from the workpiece. The wear volume values were then divided by the processing time to determine the *MRR*. Table 2 lists the corresponding heights, wear volumes, and *MRR* values for each experimental sample.

$$h = \frac{A_p}{a} \tag{1}$$

$$V = \frac{\pi l^2}{4} h \tag{2}$$

Table 1. Set values of independent variables used in the experiments and corresponding *MRR* and *TWR* values.

Exp. No	Powder Concentration (g/l)	Current (A)	T_{on} (µs)	T_{of} (µs)	*MRR* (mm³/min)	*TWR* (mm³/min)
E1	0	9	180	18	0.027	0.000
E2	0	12	240	24	0.105	0.253
E3	0	15	300	30	0.304	0.759
E4	0	18	360	36	0.506	1.266
E5	2	9	240	30	0.102	0.158
E6	2	12	180	36	0.165	0.380
E7	2	15	360	18	0.513	0.886
E8	2	18	300	24	0.586	1.138
E9	5	9	300	36	0.017	0.759
E10	5	12	360	30	0.241	1.139
E11	5	15	180	24	0.311	1.266
E12	5	18	240	18	0.350	1.425
E13	8	9	360	24	0.020	0.506
E14	8	12	300	18	0.110	1.013
E15	8	15	240	36	0.215	1.139
E16	8	18	180	30	0.223	1.899

To determine *TWR*, the electrodes to be used in each experimental process were weighed using a precision scale after which the processing was carried out for 10 minutes using the powder ratio and EDM parameters specified in Table 1. Subsequently, each electrode was re-weighed using the same scale to find their mass losses. Equation 3 was used to calculate the volume loss from the mass loss, and this value was divided by the processing time to calculate *TWR*. In Equation 3, *V* represents the volume loss, *m* stands for the mass loss, and φ represents the specific mass of the electrode. The mass

before and after each experiment, mass and volume losses, and *TWR* values for each experimental sample are listed in Table 2.

$$V = \frac{m}{\varphi} \tag{3}$$

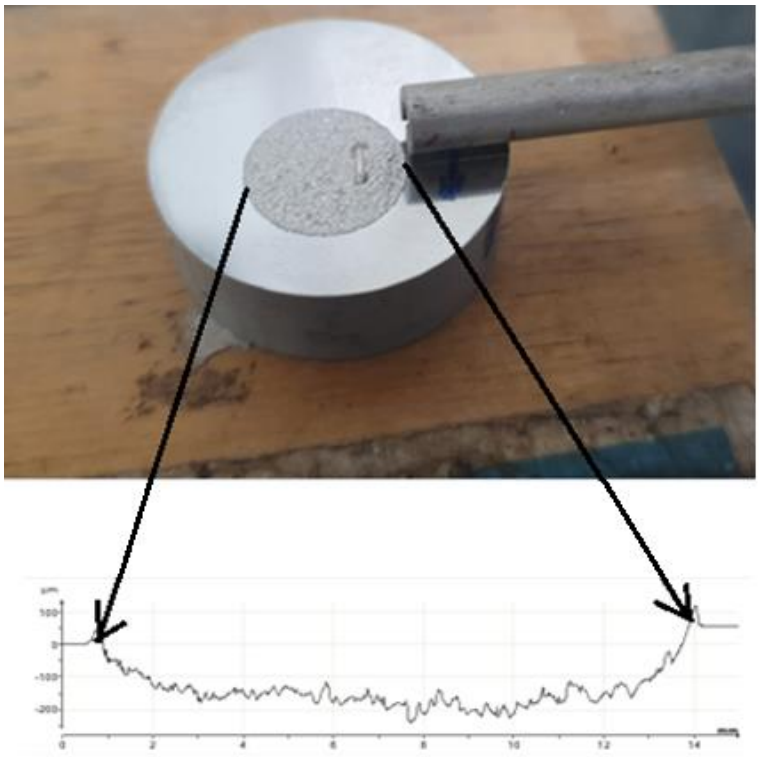

Figure 1. Obtaining wear profiles

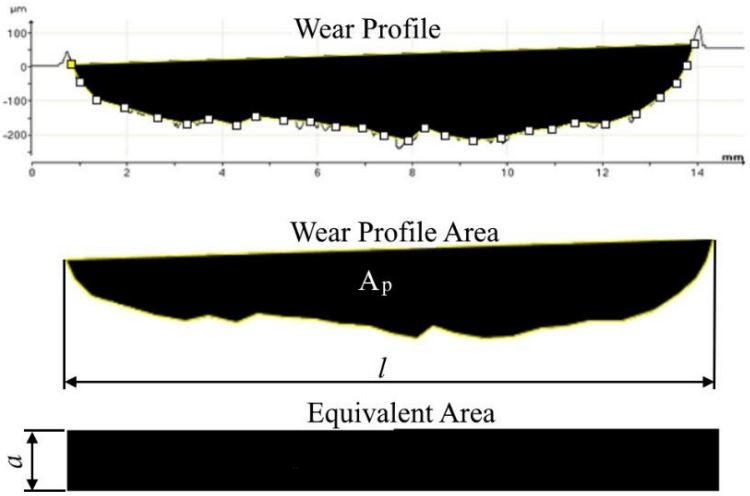

Figure 2. Calculation of equivalent height (h)

2.2 Development of Response Surfaces

In this study, the response surface methodology, which comprises statistical and mathematical operations commonly used to obtain regression models, was employed. Independent variables were set as *w*, *I*, T_{on}, and T_{off}, while the values presented in Table 1 were used to predict the dependent variables, *MRR* and *TWR*.

The Design Expert commercial software was employed in creating the response surfaces. Linear regression models were established for both *MRR* and *TWR*.

Table 2. Data to calculate *MRR* and *TWR* for each experiment sample

	Workpiece			Electrode				
Exp. No	**Equivalent Depth (µm)**	**Wear Volume (mm^3)**	***MRR* (mm^3/min)**	**Mass before process (g)**	**Mass after process (g)**	**Mass loss (g)**	**Wear volume (mm^3)**	***TWR* (mm^3/min)**
E1	23.94	0.271	0.027±0,002	121.320	121.320	0.000	0.000	0.000
E2	92.87	1.050	0.105±0,006	118.790	118.770	0.02	2.532	0.253
E3	118.31	1.337	0.134±0,009	118.560	118.500	0.06	7.595	0.759
E4	447.92	5.063	0.506±0,021	120.100	120.000	0.1	12.658	1.266
E5	90.37	1.022	0.102±0,004	121.580	121.568	0.012	1.575	0.158
E6	146.34	1.654	0.165±0,011	115.080	115.050	0.03	3.797	0.380
E7	783.04	8.851	0.885±0,041	122.430	122.360	0.07	8.861	0.886
E8	943.30	10.663	1.066±0,047	122.600	122.510	0.090	11.384	1.138
E9	15.29	0.173	0.017±0,003	120.940	120.880	0.06	7.595	0.759
E10	213.12	2.409	0.241±0,017	118.490	118.400	0.09	11.392	1.139
E11	274.8	3.106	0.311±0,015	118.160	118.060	0.1	12.658	1.266
E12	309.65	3.500	0.350±0,021	119.650	119.537	0.113	14.251	1.425
E13	17.49	0.198	0.020±0,001	121.300	121.260	0.04	5.063	0.506
E14	97.42	1.101	0.110±0,006	114.630	114.550	0.08	10.127	1.013
E15	189.91	2.147	0.215±0,013	122.110	122.020	0.09	11.392	1.139
E16	197.10	2.228	0.223±0,010	122.190	122.040	0.15	18.987	1.899

3. RESULTS AND DISCUSSION

3.1 ANOVA Results

The results of the analysis of variance (ANOVA) conducted for *MRR* and *TWR* regression models are presented in Table 3. In the table, having an F-value of around 18 for both *MRR* and *TWR*, along with model P-values of 0.0001, indicates that the models are statistically significant. Furthermore, the correlation coefficient (R2) for the *MRR* and *TWR* models is 0.8713 and 0.8697, respectively. This suggests that both models have a good level of predictive capability.

Table 3. ANOVA table for *MRR* and *TWR* models

Response	***MRR* (mm3/min)**	***TWR* (mm3/min)**
Model Type	Linear	Linear
Model Degree of Freedom	4	4
Model F-value	18,62	18,36
Model p-value	<0.0001	<0.0001
R^2	0.8713	0.8697
R^2_{adj}	0.8245	0.8224

Additionally, the adjusted R^2 (R^2_{adj}) values in the table show that the difference between R^2 and R^2_{adj} in the respective models is less than 20%. This indicates that there are no unnecessary terms in the models.

In Table 4, the coded and actual coefficients of terms for the *MRR* regression model are listed. The coded coefficients indicate the degree of influence of the terms on the dependent variables. From Table 4, it can be observed that the term *I* has the most significant impact on *MRR*, while the influence of T_{off} is relatively low. Furthermore, it is evident that *I* and *Ton* have a positive effect on *MRR*, while *w* and T_{off} have a negative impact.

Using the actual coefficients of the terms in Table 4, the *MRR* regression model is constructed as shown in Equation 4.

Table 1. Regression coefficients of coded and actual terms of *MRR* model

Terms	**Coefficients of coded terms**	**Coefficients of actuals terms**
Constant	0.2289	-0.456422
w	-0.0397	-0.016684
I	0.1163	0.04348
T_{on}	0.0425	0.000795
T_{off}	-0.0098	-0.001833

$$TWR = -4564 - 0.016684w + 0.04348I + 0.000795T_{on} - 0.001833T_{off} \quad (4)$$

The experimental values of *MRR* and the corresponding predictions from the regression model are visualized in Figure 3. It is evident from the figure that the predictions from the regression model closely match the actual values, indicating a good fit of the model to the experimental data.

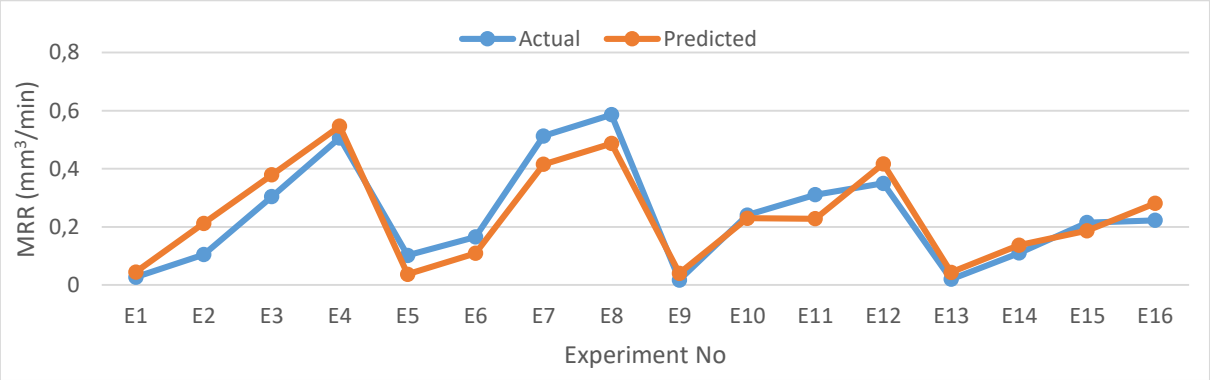

Figure 3. Measured *MRR* values and corresponding predicted values by regression model

The coded and actual coefficients of terms for the *TWR* regression model are provided in Table 5. From the coded coefficients in the table, it can be understood that all terms have a positive influence on *TWR*. Additionally, it is observed that the factor with the highest impact on *TWR* is *I*, and unlike *MRR*, the contribution of T_{off} is higher than *Ton*.

Table 5. Regression coefficients of coded and actual terms of *TWR* model

Terms	Coefficients of coded terms	Coefficients of actuals terms
Constant	0.916	-1.33361
w	0.1854	0.077966
I	0.3192	0.119312
T_{on}	0.0335	0.000625
T_{off}	0.0314	0.005862

The *TWR* regression model equation, created using the actual coefficients from Table 5, is provided in Equation 5.

$$TWR = -1.3336 + 0.07797w + 0.119312I + 0.000625T_{on} + 0.005862T_{off} \quad (5)$$

The experimental values of *TWR* and the predictions from the regression model are depicted in Figure 4. From the graph, it is evident that the model predictions closely align with the experimental results, indicating a strong agreement between the model and the actual data.

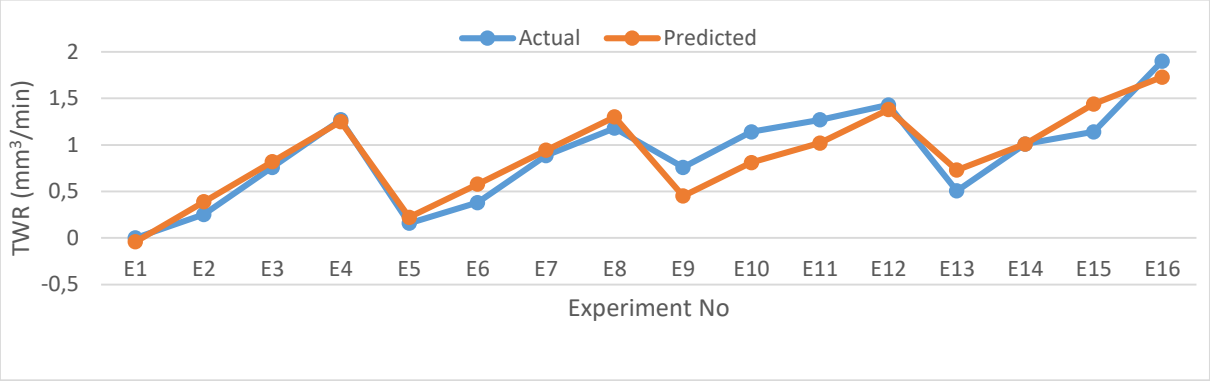

Figure 4. Measured *TWR* values and corresponding predicted values by regression model

3.2 Discussions

To gain a better understanding of how material removal rate and tool wear rate change depending on four different factors, regression models were employed to create three-dimensional surface plots. In three-dimensional plots, only one dependent variable can be represented against two independent variables at a time. Therefore, in each drawing, the values of two variables were held constant.

In Figure 5, we can observe how variations in powder ratio and discharge current relate to different constant values of *Ton* and T_{off}. In Figure 5a, when *Ton* and T_{off} are held at 210 µs and 21 µs, respectively, a linear increase in *MRR* is evident as the current is raised from 10 A to 18 A. This change is notable in the region where the powder ratio is zero, going from 0.11 mm³/min to 0.45 mm³/min, and in the region with a powder ratio of 8 g/l, where it increases from 0 to 0.32 mm³/min. As the discharge current increases, the flow of electrons between the electrode and the workpiece is expected to increase, leading to an anticipated rise in spark frequency and energy. This, in turn, will result in an increased amount of material removed from the workpiece per unit time (Elsiti & Noordin, 2017; Long, Phan, Cuong, & Jatti, 2016; Long, Phan, Cuong, & Toan, 2016; Rehman et al., 2022). Conversely, as the powder ratio increases from 0 to 8 g/l, *MRR* shows a linear decrease. This decline is noticeable, dropping from 0.11 mm³/min to 0 mm³/min when *I* is at 10 A, and from 0.45 mm³/min to 0.32 mm³/min when *I* is at 18 A. The negative impact of the powder ratio on MRR does not align

with the results in the literatüre (Banh et al., 2016; Jahan et al., 2010; Jailani et al., 2020; Majid & Issa, 2014; Razak et al., 2015; Rehman et al., 2022; Singh et al., 2015; Zain et al., 2012). This discrepancy suggests that an increase in the powder ratio may enhance wear on the electrode and that detached particles could potentially adhere to the workpiece. When we consider these changes together, it becomes apparent that the increase in *w* diminishes the positive impact of *I* on *MRR*.

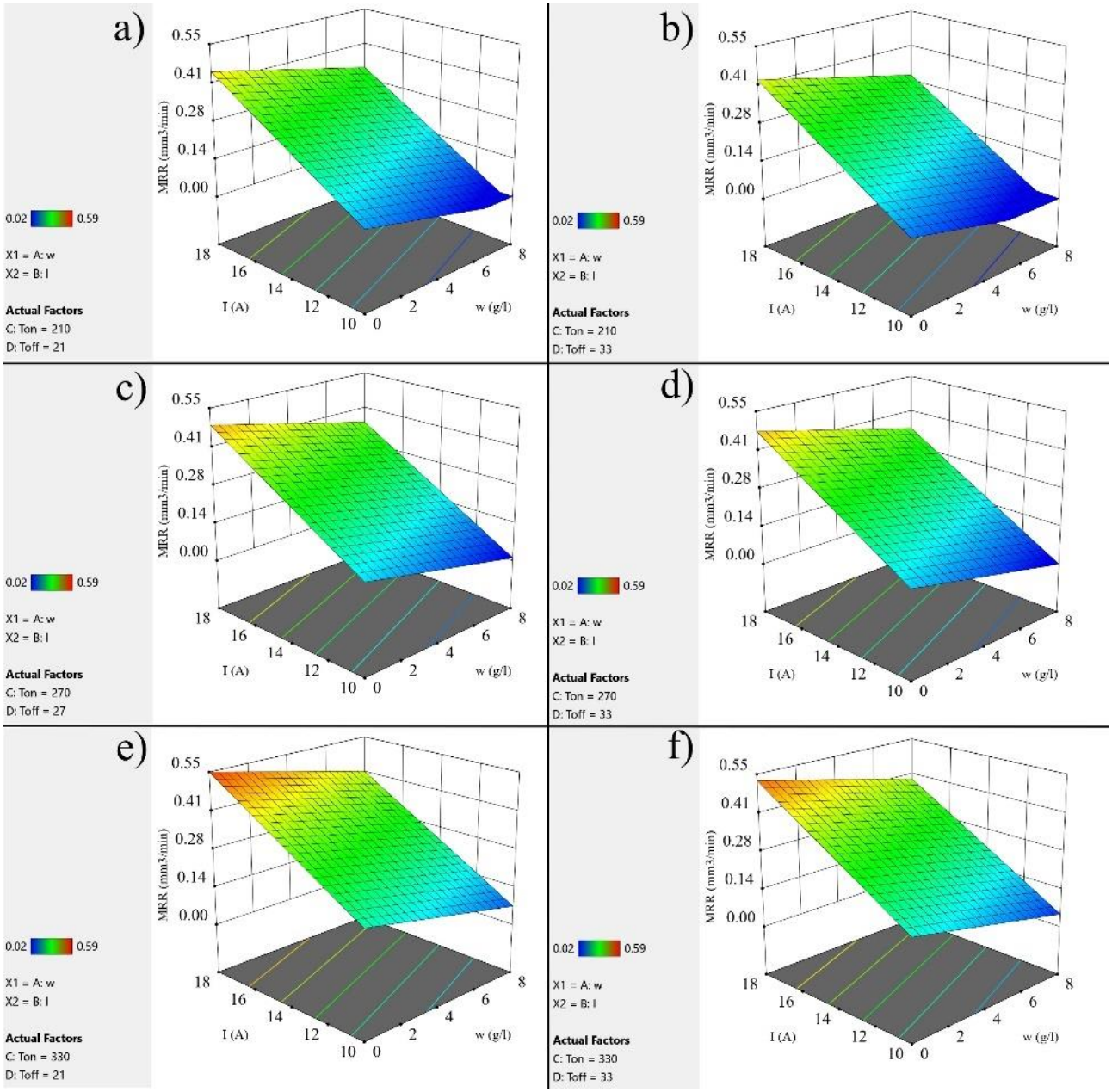

Figure 1. Change in *MRR* according to *w* and *I* for the constant values of a) T_{on} =210 µs, T_{off}=21 µs; b) T_{on} =210 µs, T_{off} =33 µs; c) T_{on} =270 µs, T_{off} =27 µs; d) T_{on} =270 µs, T_{off} =33 µs; e) T_{on} =330 µs, T_{off} =21 µs; f) T_{on} =330 µs, T_{off} =33 µs

In Figure 5b, with *Ton* and T_{off} held at fixed values of 210 ms and 33 ms, respectively, we observe a behavior closely resembling that of Figure 5a. In this graphical representation, it becomes evident that an increase in the value of T_{off} has a discernible negative impact on *MRR* across various values of *w* and *I*. These findings are consistent with those in the literature (Cuong et al., 2020; Long, Phan, Cuong, & Toan, 2016; Nguyen et al., 2021). Furthermore, at elevated *w* values, the influence of *I* appears to slightly weaken, while conversely, at higher *I* values, the effect of *w* also exhibits a marginal increase.

When *Ton* and T_{off} values are increased to their average values for the region of the study, which are 270 and 27 µs, respectively (Figure 5c), the graph exhibits a structure similar to the previous ones, and *MRR* continues to increase for all data points. Furthermore, at low *w* values, the influence of *I* appears to persistently intensify, while at high *I* values, the effect of *w* also continues to increase.

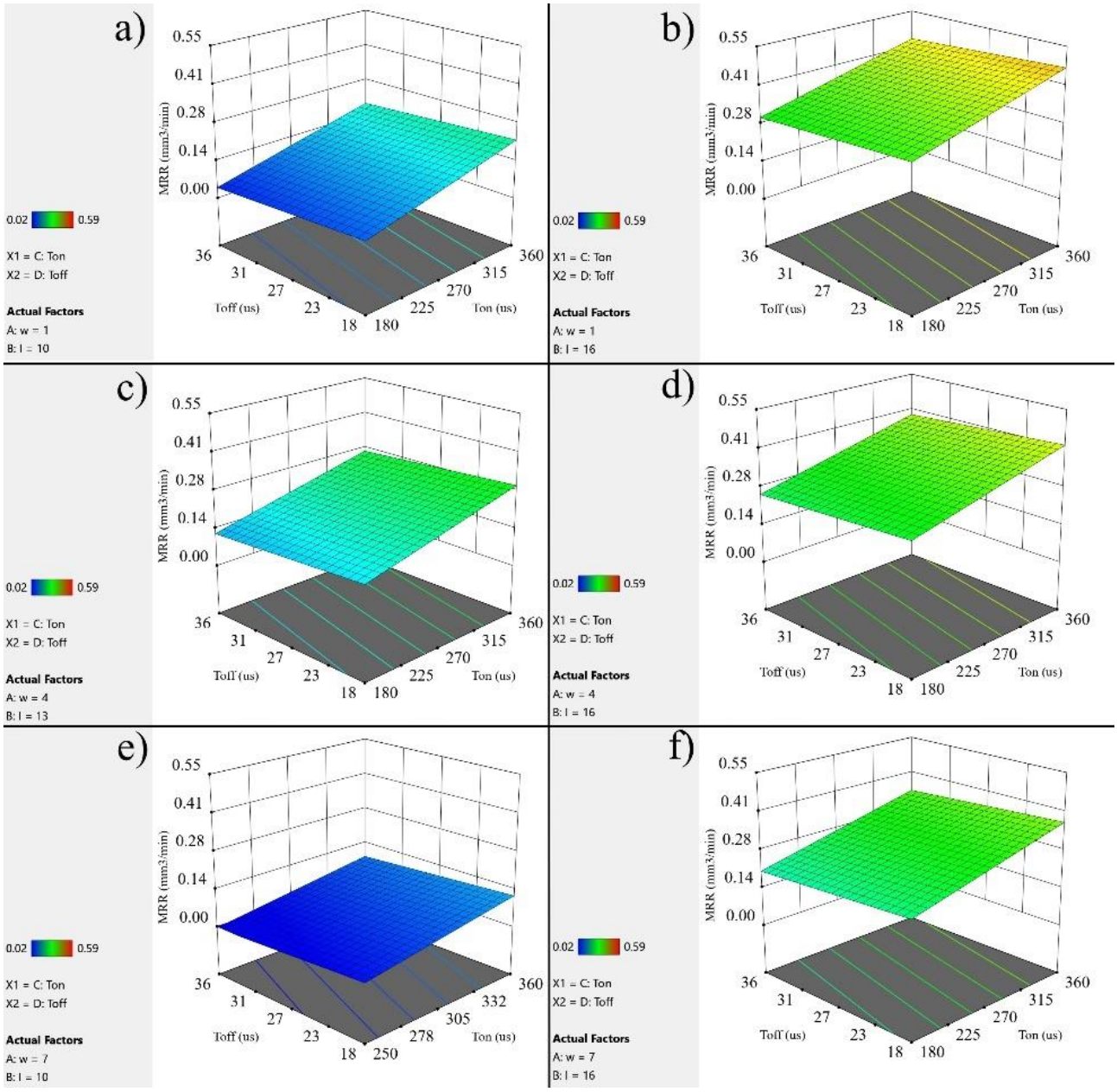

Figure 6. Change in *MRR* according to T_{on} and T_{off} for the constant values of a) *w*=1 g/l, *I*=10 A; b) *w*=1 g/l, *I*=19 A; c) *w*= 4 g/l, *I*=13 A; d) *w*=4 g/l, *I*=16 A; e) *w*=7 g/l, *I*=10 A; f) *w*=7 g/l, *I*=16 A

Figure 5c illustrates the ongoing effect of increasing T_{off} values. Beyond this point, in Figure 5d (*Ton* = 270 and T_{off} = 33 µs), the situation begins to reverse, and *MRR* is observed to decrease indistinctly across the entire graph.

In Figure 5e, at fixed values of *Ton* and T_{off}, 330 and 21 µs, respectively, *MRR* reaches its highest value at 0.548 mm³/min. Figure 5f (*Ton* = 330 and T_{off} = 33 µs) shows a slight decrease in *MRR* across the entire graph due to a slight increase in T_{off}.

The graphs illustrating the variation of *MRR* with respect to *Ton* and T_{off} for constant powder ratio and current values are presented in Figure 6. In Figure 6a, with *w* and *I* fixed at 1 g/l and 10 A,

respectively, *MRR* linearly increases from 0.072 mm³/min to 0.214 mm³/min as *Ton* increases from 180 to 360 µs when T_{off} is 18 µs. In the region where T_{off} is 36 µs, *MRR* similarly rises from 0.039 mm³/min to 0.181 mm³/min within the same *Ton* range. This suggests that the rate of change remains constant for the same T_{off} values.

Upon comprehensive examination of Figure 6a, b, c, d, e, and f, it becomes evident that the increases in current lead to an augmentation of *MRR* across all areas covered by the graphs. Conversely, an increase in the powder ratio is discerned to reduce *MRR* across the entire dataset. Furthermore, with an increase in current (*I*), the slope of *MRR* concerning *Ton* at constant T_{off} values also escalates.

In Figure 7, variation graphs of *TWR* with respect to powder ratio and discharge current for different fixed values of *Ton* and T_{off} are depicted. In Figure 7a, the alterations in *TWR* with respect to *w* and *I* at values of *Ton* and T_{off}, namely, 210 µs and 21 µs, are presented in three dimensions. The graph illustrates that, in the region where *w* equals 0 and *I* ranges from 9 to 18 A, *MRR* linearly increases from 0 to 1.07 mm³/min. When the powder ratio reaches 8 g/l, the change in *MRR* within the *I* range of 9 to 18 A is observed to elevate from 0.77 mm³/min to 1.83 mm³/min. The increase in energy resulting from the rise in discharge current will lead to an increase in temperature not only on the workpiece surface but also on the tool surface, consequently causing an escalation in tool wear (Joshi & Joshi, 2021; Oskueyan et al., 2022; S. et al., 2018).

Conversely, in the region where *I* is 9 A, when *w* increases from 0 to 8 g/l, *TWR* has risen from 0.14 mm³/min to 0.76 mm³/min. This change is observed to occur as an increase from 1.21 mm³/min to 1.84 mm³/min when *I* reaches 18 A. The increase in the powder ratio leading to the rise in TWR is in line with the influence of graphite powder observed in Çogun et al.'s study (Çogun et al., 2006; Jahan et al., 2010).

Upon examining all the graphs in Figure 7 collectively, it becomes apparent that they share a remarkably similar pattern, with *TWR* values exhibiting a gradual and indistinct rise with the increase of *Ton* and T_{off}.

The variation of *MRR* with *Ton* and T_{off} at different fixed values of powder ratio and discharge current is illustrated in Figure 8 through three-dimensional graphs.

In Figure 8a, the variations of *TWR* with respect to *Ton* and T_{off} are depicted with *w* fixed at 1 g/l and *I* at 10 A. In the region where T_{off} is 18 ms, an increase in *Ton* from 180 ms to 360 ms results in a linear rise of *MRR* from its lowest value of 0.16 mm³/min to 0.27 mm³/min. In the same region of T_{off} at 18 ms, this change takes place as an elevation from 0.26 mm³/min to the highest value in the graph, which is 0.37 mm³/min.

The changes in *TWR* in the other graphs closely resemble that of Figure 8a. In each graph, while the values of *TWR* vary with *w* and *I*, the slopes remain consistent. In Figure 8a, with *w* at 1 g/l and *I* at 10 A, the minimum and maximum *TWR* values are 0.17 and 0.37 mm³/min, respectively. In Figure 8c, with *w* at 7 g/l and *I* at 10 A, these values increase to 0.62 and 0.84 as *I* increases. On the other hand, with *I* fixed at 16 A, while *w* varies at 1 g/l (Figure 8b), 4 g/l (Figure 8d), and 7 g/l (Figure 8c), the minimum and maximum *TWR* values are determined as 0.87 and 1.08; 1.11 and 1.32; and 1.34 and 1.45, respectively. From this, it can be inferred that the influence of *I* on *TWR* is significantly higher than that of *w*.

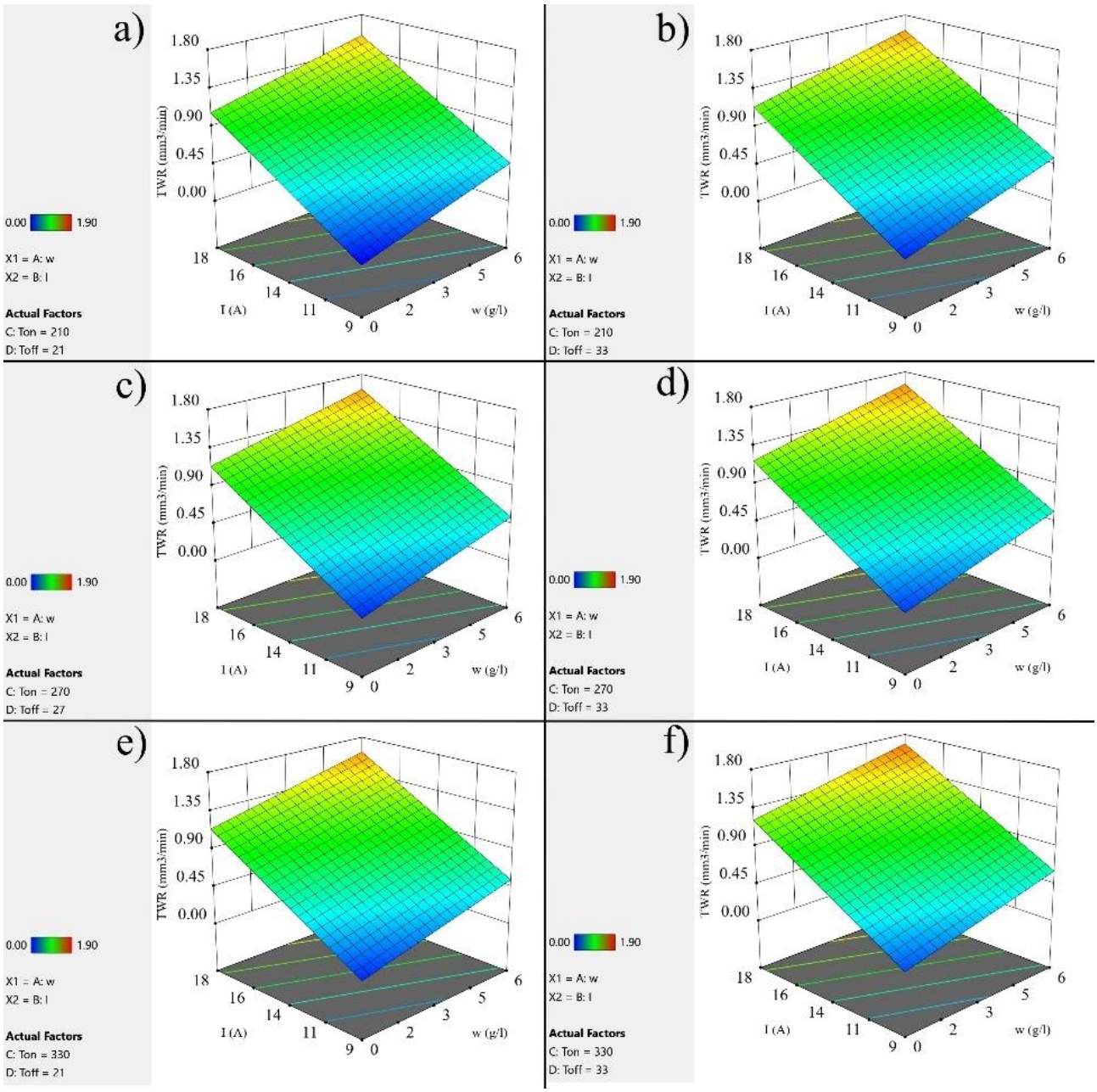

Figure 7. Change in *TWR* according to *w* and *I* for the constant values of a) T_{on} =210 µs, T_{off} =21 µs; b) T_{on} =210 µs, T_{off} =33 µs; c) T_{on} =270 µs, T_{off} =27 µs; d) T_{on} =270 µs, T_{off} =33 µs; e) T_{on} =330 µs, T_{off} =21 µs; f) T_{on} =330 µs, T_{off} =33 µs

4. CONCLUSION

In the present study, RSM was used to model the effect of EDM parameters on *MRR* and *TWR* during the machining of a CoCr28Mo6 workpiece with an AISI 316L electrode and a Ti6V4Al dielectric liquid additive at different ratios. Linear response surfaces constructed by using experimental results of experimental machining of the sample with variable set values of the variables.

Linear regression models developed for *MRR* and *TWR* with R^2 of 0.8713 and 0.8697 respectively. Significances of the models are also verified by p-values smaller than 0.0001.

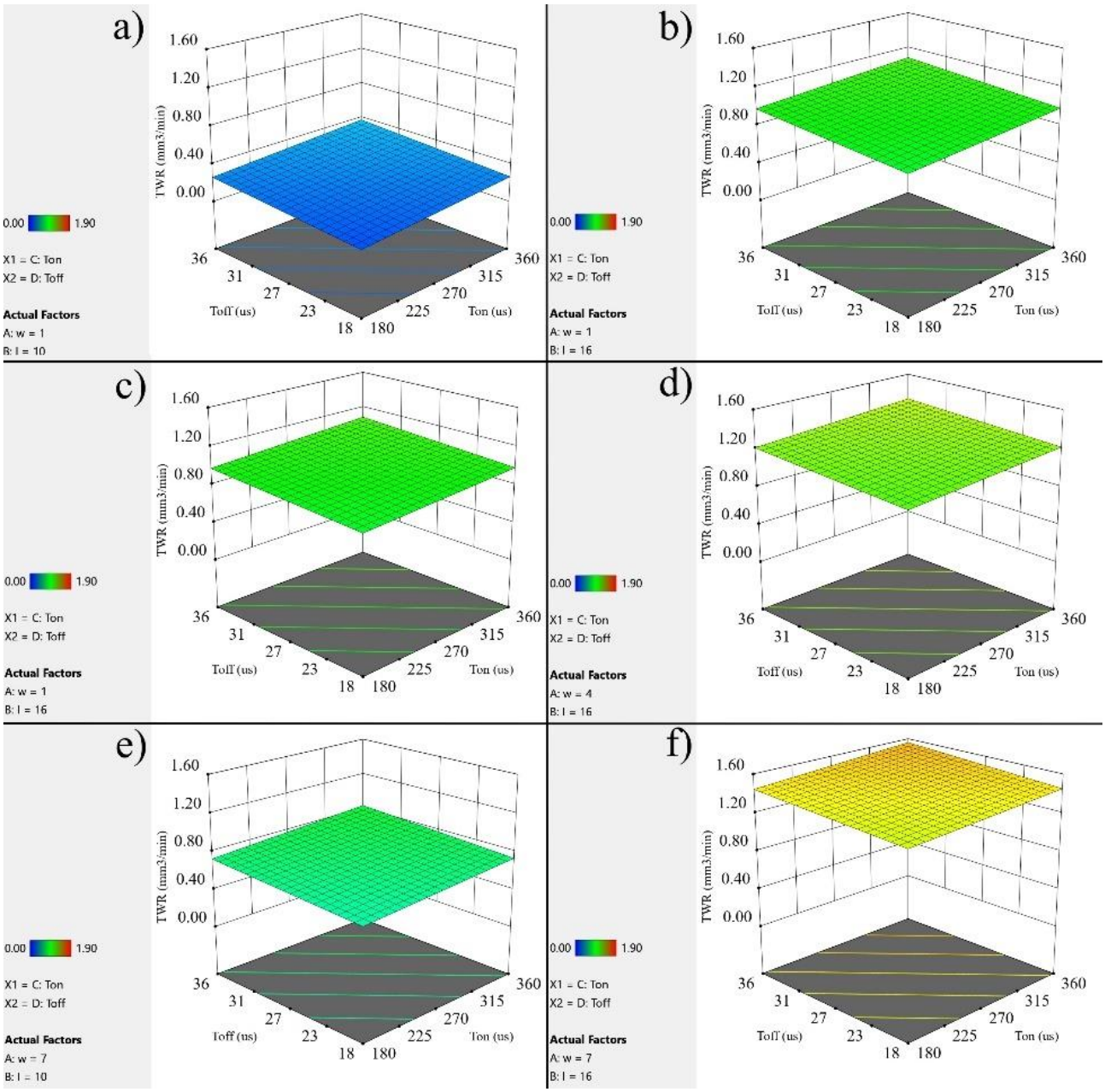

Figure 8. Change in *MRR* according to T_{on} and T_{off} for the constant values of a) *w*=1 g/l, *I*=10 A; b) *w*=1 g/l, *I*=10 A; c) *w*=1 g/l, *I*=10 A; d) *w*=1 g/l, *I*=10 A; e) *w*=1 g/l, *I*=10 A; f) *w*=1 g/l, *I*=10 A

Response surfaces plotted in 3-D according to the mathematical models of *MRR* and *TWR* and following items have been concluded from these plots.

- The most effective factor on *MRR* is *I*. The order of significance of the other factors is as follows: *Ton*, *w*, and T_{off}.
- Impact of *I* and *Ton* on *MRR* is positive, while that of *w* and T_{off} is negative.
- At high dust concentrations, the impact of *I* on *MRR* slightly decreases.
- Effect of *w* on *MRR* increases at higher *I* values.
- *I* is the most influential factor on *MRR*. Additionally, *w* also has a significant effect. However, the influence of *Ton* and T_{off} on *TWR* is quite limited.
- All of the factors have positive impact on *TWR*.

5. ACKNOWLEDGEMENTS

We would like to thank the Payas Vocational and Technical Anatolian High School Directorate for their support.

6. CONFLICT OF INTEREST

Authors approve that to the best of their knowledge, there is not any conflict of interest or common interest with an institution/organization or a person that may affect the review process of the paper.

7. AUTHOR CONTRIBUTION

Faruk ÇAVDAR performed experiment design, constructed response surface models, constructed and interpreted of *MRR* and *TWR* plots, prepared the manuscript. Can YILDIZ manufactured of experiment set up, prepared workpiece samples and electrodes, conducted of experimental machining, made critical analysis of the manuscript. Erdoğan KANCA determined the concept, designed process of the research, and managed the research, obtained of surface profiles, determined of *MRR* and *TWR* values, made critical analysis of the manuscript.

8. REFERENCES

Abbas M.A., Lajis M.A., Abbas D.R., Merzah O.M., Kadhim M.H., Shamran A.A., Influence of additive materials on the roughness of AISI D2 steel in electrical discharge machining (EDM) environment. Materialwissenschaft Und Werkstofftechnik 51(6), 719–724, 2020.

Abdudeen A., Abu Qudeiri J.E., Kareem A., Ahammed T., Ziout A., Recent Advances and Perceptive Insights into Powder-Mixed Dielectric Fluid of EDM. Micromachines 11(8), 754, 2020.

Al-Amin M., Abdul-Rani A.M., Aliyu A.A., Bryant M., Danish M., Ahmad A., Bio-ceramic coatings adhesion and roughness of biomaterials through PM-EDM: a comprehensive review. Materials and Manufacturing Processes 35(11), 1157-1180, 2020.

Al-Amin M., Abdul-Rani A.M., Danish M., Rubaiee S., Mahfouz A.bin, Thompson H.M., Ali S., Unune D.R., Sulaiman M.H., Investigation of Coatings, Corrosion and Wear Characteristics of Machined Biomaterials through Hydroxyapatite Mixed-EDM Process: A Review. Materials 14(13), 3597, 2021.

Bahçe E., Aslan A.K., Çakır N., Güler M.S., CoCrMo Alaşımı Üzerine TaN Esaslı İnce Film Kaplamaların Yüzey Özelliklerinin İncelenilmesi. Karadeniz Fen Bilimleri Dergisi 9(2), 223–237, 2019.

Bains P.S., Bahraminasab M., Sidhu S.S., Singh G., On the machinability and properties of Ti–6Al–4V biomaterial with n-HAp powder–mixed ED machining. Proceedings of the Institution of Mechanical Engineers, Part H: Journal of Engineering in Medicine 234(2), 232–242, 2020.

Banh L.T., Nguyen P.H., Ngo C., Tool wear rate optimization in PMEDM using titanium powder by Taguchi method for die steels. Science and Technology Development Journal 19(2), 88–97, 2016.

Cakıroglu R., Investigation of The Effects of Processing Parameters on Measuring Accuracy in Electro Erosion Machining of Ti-6Al-4V Alloy. Gazi Üniversitesi Fen Bilimleri Dergisi Part C: Tasarım ve Teknoloji, 10(1), 77–85, 2022.

Ceritbinmez F., Günen A., Gürol U., Çam G. A comparative study on drillability of Inconel 625 alloy fabricated by wire arc additive manufacturing. Journal of Manufacturing Processes 89, 150–169, 2023.

Ceritbinmez F., Kanca E., The Effects of Cutting Parameters on the Kerf and Surface Roughness on the Electrode in Electro Erosion Process. Gazi Üniversitesi Fen Bilimleri Dergisi Part C: Tasarım ve Teknoloji 9(2), 335–346, 2021.

Ceritbinmez F., Kanca E., The Effects of Using Brass and Copper Wires on the Cutting Quality of Sleipner Cold Work Steel Cut by WEDM. Journal of Materials and Mechatronics: A 3(2), 163–178, 2022.

Chakmakchi M., Ntasi A., Mueller W.D., Zinelis S., Effect of Cu and Ti electrodes on surface and electrochemical properties of Electro Discharge Machined (EDMed) structures made of Co-Cr and Ti dental alloys. Dental Materials 37(4), 588–596, 2021.

Cuong N.M., Tung L.A., Danh B.T., Cuong N., Van, Hong T.T., Linh N.H., Quy L.T., Pi V.N., Influence of Input Factors on Material Removal Rate in PMEDM Cylindrical Shaped Parts with Silicon Carbide Powder Suspended Dielectric. Key Engineering Materials 861, 129–135, 2020.

Çogun C., Özerkan B., Karaçay T., An experimental investigation on the effect of powder mixed dielectric on machining performance in electric discharge machining. Proceedings of the Institution of Mechanical Engineers, Part B: Journal of Engineering Manufacture 220(7), 1035–1050, 2006.

Elsiti N., Mohd Yusof N., Idris A., Effect of maghemite (γ-Fe2O3) nano-powder mixed dielectric medium on tool wear rate (*TWR*) during micro-EDM of CO-Cr-MO. Pertanika Journal of Science and Technology 25, 847–858, 2017.

Elsiti N.M., Noordin M.Y., Experimental Investigations into the Effect of Process Parameters and Nano-Powder (Fe2O3) on Material Removal Rate during Micro-EDM of Co-Cr-Mo. Key Engineering Materials 740, 125–132, 2017.

Erdem O., Kılıç S., TiO2 Katkılı Çevre Dostu Dielektrik Sıvının Elektro Erozyon Delik Delme Performanslarının Araştırılması. Bilecik Şeyh Edebali Üniversitesi Fen Bilimleri Dergisi 7 (2), 863-885, 2020.

Ho K.H., Newman S.T., State of the art electrical discharge machining (EDM). International Journal of Machine Tools and Manufacture 43(13), 1287–1300, 2003.

Iranmanesh S., Esmaeilzadeh A., Razavykia A., Optimization of Electrical Discharge Machining Parameters of Co-Cr-Mo Using Central Composite Design. Campana, G., Howlett, R., Setchi, R., Cimatti, B. (eds) Sustainable Design and Manufacturing 2017. SDM 2017. Smart Innovation, Systems and Technologies, vol 68. Springer, 48–57, 2017.

Jahan M.P., Rahman M., Wong Y.S., Modelling and experimental investigation on the effect of nanopowder-mixed dielectric in micro-electrodischarge machining of tungsten carbide. Proceedings of the Institution of Mechanical Engineers, Part B: Journal of Engineering Manufacture 224(11), 1725–1739, 2010.

Jailani H.S., Murugan M., Jeavudeen S., Powder additives influence on dielectric strength of EDM fluid and material removal. International Journal of Machining and Machinability of Materials 22(1), 47, 2020.

Jakobsen S.S., Baas J., Jakobsen T., Soballe K., Acid Etching does not Improve CoCrMo Implant Osseointegration in a Canine Implant Model. HIP International 20(2), 171–178, 2010.

Jawahar M., Sridhar Reddy Ch., Srinivas Ch., A review of performance optimization and current research in PMEDM. Materials Today: Proceedings 19, 742–747, 2019.

Joshi A.Y., Joshi A.Y., Multi response optimization of PMEDM of Ti6Al4V using Al2O3 and SiC powder added de-ionized water as dielectric medium using grey relational analysis. SN Applied Sciences 3(7), 718, 2021.

Kayalı Y., Yalçın, Y., Borlanmış AISI 316 L Paslanmaz Çeliğin Difüzyon Kinetiğinin İncelenmesi . Journal of Materials and Mechatronics: A 1(1), 12–21, 2020.

Kumar S., Multi Objective Optimization of Process Parameters of EDM on EN 31 Alloy Steel by Using Grey-Taguchi Method. International Journal for Research in Applied Science and Engineering Technology 6(4), 4771–4778, 2018.

Kumar S.S., Erdemir F., Varol T., Kumaran S.T., Uthayakumar M., Canakci A., Investigation of WEDM process parameters of Al–SiC–B4C composites using response surface methodology. International Journal of Lightweight Materials and Manufacture 3(2), 127–135, 2020.

Long B.T., Phan N.H., Cuong N., Jatti V.S., Optimization of PMEDM process parameter for maximizing material removal rate by Taguchi's method. The International Journal of Advanced Manufacturing Technology 87(5–8), 1929–1939, 2016.

Long B.T., Phan N.H., Cuong N., Toan N.D., Surface quality analysis of die steels in powder-mixed electrical discharge machining using titan powder in fine machining. Advances in Mechanical Engineering 8(7), 168781401665773, 2016.

Long M., Rack H.J., Titanium alloys in total joint replacement—a materials science perspective. Biomaterials 19(18), 1621–1639, 1998.

Mahajan A., Sidhu S. S., Ablyaz T., EDM Surface Treatment: An Enhanced Biocompatible Interface. In P. S. Bains, S. S. Sidhu, M. Bahraminasab C. Prakash (Eds.), Biomaterials in Orthopaedics and Bone Regeneration: Design and Synthesis, Springer Singapore, 33–40, 2019.

Mahajan A., Sidhu S.S., Potential of electrical discharge treatment to enhance the in vitro cytocompatibility and tribological performance of Co–Cr implant. Journal of Materials Research 34(16), 2837–2847, 2019b.

Mahajan A., Sidhu, S.S., In vitro corrosion and hemocompatibility evaluation of electrical discharge treated cobalt–chromium implant. Journal of Materials Research, 34(8), 1363–1370, (2019a).

Majid M.A., Issa A.M., Effect of electric discharge machining of die steel DIN 1.2714 and DIN 1.2343 on surface characteristics and performance measures, 565–577, 2014.

Mujumdar S.S., Curreli D., Kapoor S.G., Ruzic D. Modeling of Melt-Pool Formation and Material Removal in Micro-Electrodischarge Machining. Journal of Manufacturing Science and Engineering 137(3), 2015.

Nguyen A.T., Le X.H., Nguyen V.T., Phan D.P., Tran Q.H., Nguyen D.N., Nguyen M.C., Vu N.P., Optimizing Main Process Parameters When Conducting Powder-Mixed Electrical Discharge Machining of Hardened 90CrSi. Machines, 9(12), 375, 2021.

Onderka F., Volodarskaja A., Kadlec J., Dobrocký D., Klanica O., Electrochemical Deposition of Hydroxyapatite Coatings on CoCrMo Alloy. ECS Transactions 63(1), 277–289, 2014.

Oskueyan S., Abedini V., Hajialimohammadi A., Effects of hybrid Al2O3 - SiO2 nanoparticles in deionized water on the removal rate and surface roughness during electrical discharge machining of Ti-6Al-4V. Proceedings of the Institution of Mechanical Engineers, Part E: Journal of Process Mechanical Engineering 236(3), 1122–1133, 2022.

Öztürk O., Türkan U., Eroglu, A.E., Metal ion release from nitrogen ion implanted CoCrMo orthopedic implant material. Surface and Coatings Technology 200(20–21), 5687–5697, 2006.

Peng P.W., Ou K.L., Lin H.C., Pan Y.N., Wang C.H. Effect of electrical-discharging on formation of nanoporous biocompatible layer on titanium. Journal of Alloys and Compounds, 492(1–2), 625–630, 2010.

Rajkumar H., Vishwakamra M., Performance Parameters Characteristics of PMEDM: A Review. International Journal of Applied Engineering Research 13(7), 5281-5290, 2018.

Razak M.A., Abdul-Rani A.M., Nanimina A.M., Improving EDM Efficiency with Silicon Carbide Powder-Mixed Dielectric Fluid. International Journal of Materials, Mechanics and Manufacturing 3(1), 40–43, 2015.

Rehman A.U., Arif W., Hussain M.I., Miran S., Hussain S., Lee G.H., Analysis of Particle Size and Concentration in Die Sinking Electric Discharge Machining. Materials 15(14), 4932, 2022.

S. R., Jenarthanan M.P., A.S., B.K., Experimental investigation of powder-mixed electric discharge machining of AISI P20 steel using different powders and tool materials. Multidiscipline Modeling in Materials and Structures 14(3), 549–566, 2018.

Sharma R., Singh J., Effect of Powder Mixed Electrical Discharge Machining (PMEDM) on Difficult-to-machine Materials – a Systematic Literature Review 14(4), 233–255, 2014.

Singh B., Kumar J., Kumar S., Influences of Process Parameters on MRR Improvement in Simple and Powder-Mixed EDM of AA6061/10%SiC Composite. Materials and Manufacturing Processes 30(3), 303–312, 2015.

Srivastava S., Vishnoi M., Gangadhar M.T., Kukshal, V., An insight on Powder Mixed Electric Discharge Machining: A state of the art review. Proceedings of the Institution of Mechanical Engineers, Part B: Journal of Engineering Manufacture, 237(5), 657–690, 2023.

Trajer M., Analysis of the relationship between the properties of selected materials and the parameters of the EDD process. Materials Research Proceedings 28, 1747–1758, 2023.

Yang W.E., Huang, H.H., Improving the biocompatibility of titanium surface through formation of a TiO2 nano-mesh layer. Thin Solid Films 518(24), 7545–7550, 2010.

Yıldız C., Çavdar F., Kanca E., A Response Surface Modeling Study on Effects of Powder Rate and Machining Parameters on Surface Quality of CoCrMo Processed by Powder Mixed Electrical Discharge Machining. Karadeniz Fen Bilimleri Dergisi 13(2), 415–433, 2023.

Zain Z.M., Ndaliman M.B., Khan A.A., Ali M.Y., Electro-Discharge Machining of SUS 304 Stainless Steel with TaC Powder-Mixed Dielectric. Advanced Materials Research, 576, 72–75, 2012.

Zhang W., Li L., Wang N., Meng J., Ren J., Surface modification of Ti-6Al-4 V by gas–liquid mixed EDM. The International Journal of Advanced Manufacturing Technology, 119(5–6), 3833–3844, 2022.